THE JOURNAL OF PHYSICAL CHEMISTRY C

Article

pubs.acs.org/JPCC

Surface Composition Changes of Redox Stabilized Bimetallic CoCu Nanoparticles Supported on Silica under H_2 and O_2 Atmospheres and During Reaction between CO_2 and H_2: In Situ X-ray Spectroscopic Characterization

Selim Alayoglu,[†,‡,#] Simon K. Beaumont,[†,‡,#,▽] Gérôme Melaet,[†,‡] Avery E. Lindeman,[†,‡] Nathan Musselwhite,[†,‡] Christopher J. Brooks,[§] Matthew A. Marcus,[∥] Jingua Guo,[∥] Zhi Liu,[∥] Norbert Kruse,[⊥] and Gabor A. Somorjai*[,†,‡]

[†]Department of Chemistry, University of California, Berkeley, Berkeley, California 94704, United States

[‡]Materials Sciences Division, Lawrence Berkeley National Laboratory, Berkeley, California 94720, United States

[§]Honda Research Institute, Columbus, Ohio 43212, United States

[∥]Advanced Light Source, Lawrence Berkeley National Laboratory, Berkeley, California 94720, United States

[⊥]Université Libre de Bruxelles, Chimie Physique des Matériaux, Campus de la Plaine CP 243, B-1050 Bruxelles, Belgium

Supporting Information

ABSTRACT: In this paper, we report the colloidal synthesis and detailed characterization of 11 nm bimetallic CoCu nanoparticle catalysts. Presently Co and Cu is an attractive combination because of their respective properties for industrially important Fischer−Tropsch and methanol synthesis reactions of CO (and CO_2) with H_2. We report the preparation of catalysts by deposition of bimetallic metal nanoparticles, both within mesoporous silica (MCF-17) and on the native oxide surface of a silicon wafer. Subsequent phase separation into phase-segregated (i.e., dimer) particles is found to occur upon redox treatment. These nanoparticle catalysts have then been investigated using an array of techniques including synchrotron-based ambient pressure X-ray photoelectron spectroscopy (APXPS) and in situ near edge and extended X-ray absorption fine structure (NEXAFS/EXAFS) spectroscopies. CO_2 hydrogenation is used as a probe reaction. All three techniques combine to show that an oxygen atmosphere segregates copper to the surface. In doing so the oxygen produces oxides of both Co and Cu metals. Significant hydrogen pressure and temperature are required to fully rereduce both metals to a metallic state as demonstrated by NEXAFS spectroscopy. Under the conditions of the CO_2/H_2 reaction monitored in situ using NEXAFS spectroscopy, both metals exist in a fully reduced state at 2.7 bar, 1:3 CO_2:H_2, and 260 °C.

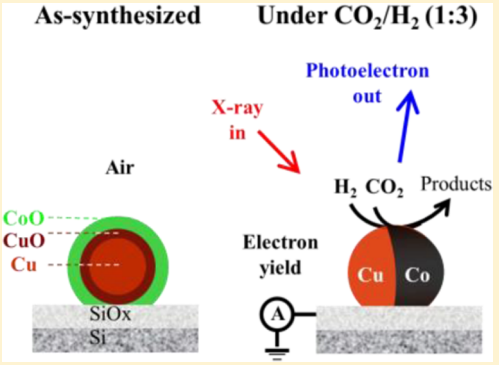

INTRODUCTION

Bimetallic nanoparticles (NPs) are often employed to improve surface activity and influence selectivity in heterogeneous catalytic processes. In particular, the bimetallic Co−Cu system has recently gained attention due to rapidly increasing interest in exploitation of Fischer−Tropsch synthesis.[1] This process helps tackle the problem of dwindling global oil reserves by conversion of other feedstocks (natural gas, coal, and biomass) to liquid hydrocarbon "oil-like" products (following initial gasification to syngas, CO + H_2). A number of studies have highlighted the potential of using CoCu in this area.[2−6] The underlying motivation for using CoCu as a Fischer−Tropsch catalyst is to obtain more C_{2+} alcohols in the product stream, which would be highly desirable in the production of transport fuels. In a detailed screen of CuCoCr industrial catalysts, selectivity toward C1−C6 alcohols for a catalyst comprising predominantly Cu and Co was reported (although the molecular level structure of the material was not well understood).[7] Similarly, the use of Co and Cu in combination appears in a number of patents for the manufacture of higher alcohols (with chain lengths suitable for use as additives to gasoline).[8,9] This synergy of Cu and Co can also be anticipated on the basis of their properties as single element catalysts. Cu is used (along with a ZnO cocatalyst) for methanol synthesis, while Co is used to produce long chain hydrocarbons.[10] Combining Cu with Co has therefore been anticipated to enhance the formation of higher oxygenates in the CO (or CO_2)/H_2 reaction. From a mechanistic standpoint, both metals are believed to interact with carbon monoxide differently.[11,12] On copper, CO_2 or CO tend to adsorb molecularly

Received: June 10, 2013
Revised: September 9, 2013
Published: September 25, 2013

and dissociation is slow, leading to incorporation of oxygen in the products.[11−14] In contrast cobalt adsorbs CO dissociatively in H_2 leading to the loss of oxygen as water and the separate production of oxygen free hydrocarbons.[15,16]

For bimetallic catalysts such as CoCu, understanding the activity and selectivity of the catalyst in terms of its mode of operation in reactive gases is challenging. For d-block elements like Co and Cu this is determined in part by surface ensemble effects and oxidation state changes.[17] Since these surfaces are subject to changes in their chemical, elemental and electronic structure under the pressure and temperature conditions of catalytic reactions, in situ/operando studies that evaluate the catalyst in reactive atmospheres are of utmost importance in understanding the structure of the surface upon which the reaction actually occurs. We have previously reviewed the exploitation of synchrotron-based X-ray spectroscopic techniques for studies of this kind;[18] however, several specific examples concerning methanol and Fischer−Tropsch synthesis are of particular relevance to the present study. Polycrystalline films of CuZnO have been studied using XAFS spectroscopy and APXPS during methanol synthesis from syngas, revealing that Cu remains metallic at elevated temperatures and mbar pressures.[19,20] Weckhuysen and co-workers also demonstrated that Cu promotes the reduction of Fe_2O_3 to metallic Fe in 0.4 bar of CO:H_2 (1:2) by using ambient pressure X-ray photoelectron spectroscopy (APXPS) and in situ near edge X-ray absorption fine structure (NEXAFS) spectroscopy.[21,22] The two-way effect of Cu on Co and Co on Cu in reactive atmospheres has, however, not been explored in detail previously and as discussed above is of significant importance in understanding the catalytic mechanisms of CO hydrogenation reactions over CoCu catalysts. Here, we report a detailed study combining the preparation of well-defined bimetallic CoCu nanoparticles that are stable following redox treatments and deposition within the pores of mesoporous silica (studied ex situ using TEM, EDS, and EELS), and their behavior in reactive gases studied by APXPS and in situ NEXAFS (Co and Cu L-edge) and EXAFS (Co and Cu K-edge) spectroscopy under redox atmospheres and during CO_2/H_2 reactions. CO_2 reduction (rather than CO) has been chosen as a probe reaction for two reasons. Firstly, because of the important technological precedent that it, rather than CO, is incorporated in reaction products during methanol synthesis.[23] Secondly, owing to the fact that CO_2 is more likely to result in the catalyst becoming oxidized than pure CO/H_2 and therefore offers an upper bound on the type of surface oxidation states anticipated during reaction as a result of oxidation by the product water, which is often present in synthesis gas reactions,[24] possibly especially so for CO_2 due to reverse water gas shift. This allows us to conclude that for all such reactions at relevant conditions both metals remain fully reduced.

EXPERIMENTAL SECTION

Methods. Scanning transmission electron microscopy (STEM)/energy dispersive spectroscopy (EDS) and STEM/electron energy loss spectroscopy (EELS) were conducted using a Jeol 2100F TEM equipped with an INCA EDS spectrometer and a GIF Tridiem EELS spectrometer operating at 200 and 120 kV, respectively. Point-to-point spatial resolution of the electron probe was 1.5 nm, and the fwhm of the zero loss peak (ZLP) measured in vacuum was 0.8 eV. Scanning electron microscopy (SEM) was carried out at 5 kV by using a ZEISS Ultra55 SEM. A PHI 5400 X-ray photoelectron spectroscopy (XPS) system with an Al Kα source and a Bruker D8 Discover X-ray diffraction (XRD) system with a Co K source were used for the vacuum XPS and XRD measurements, respectively.

All synchrotron studies were conducted at the Advanced Light Source, Lawrence Berkeley National Laboratory. A 2D dip-coated film of CoCu NPs on a Si substrate was used for the APXPS and soft X-ray based in situ NEXAFS spectroscopy measurements. For the EXAFS experiment, CoCu/MCF-17 catalyst powder was pressed into a thin (∼200 μm) pellet. The supported catalysts (both 2D and 3D) were conditioned at 350 °C under a flow of 20 vol. % (i) O_2 and (ii) H_2 (in He balance) for 1 h in each. APXPS was performed using beamline 9.3.2 as described elsewhere.[25] XPS data and error analysis was carried out using CasaXPS software. Soft X-ray NEXAFS spectroscopy was carried out at beamline 7.0.1 (total electron yield detection at the Co and Cu $L_{3/2}$ edges) using the in situ reaction cell described elsewhere.[26]

Hard X-ray absorption spectroscopy was conducted at beamline 10.3.2[27] using fluorescence yield detection at the Co and Cu K edges and again using an in situ cell. The in situ cell used in beamline 10.3.2 consists of a stainless steel body and a stainless steel lid with a 1 × 1 cm^2 window, which seals on the body using a Viton O-ring. A 70 μm thick Kapton membrane was hermatically sealed on the window using a silver paste. The heater components consist of a Boraelectric heater element and a K-type thermocouple, and located in the body and 3 mm below the window. The sample is placed above the heater element and in between two electrically isolated metal plates with 3 mm diameter holes in the center. The gas mixtures are delivered to the body using a gas manifold consisting of carefully calibrated mass flow controllers and a Baratron gauge.

The QuickXAS mode was utilized for data acquisition; deadtime correction, pre-edge removal and postedge normalization were carried out employing software developed for beamline 10.3.2. The Artemis software from the IFEFFIT suite was employed in data analysis.[28] The FT window was between 2 and 13.5 $Å^{-1}$. The theoretical reference data was calculated from the cubic metallic or oxide crystal structures ($Fm\bar{3}m$) by using the IFEF6 code. Attempts to use the EXAFS data to obtain reliable information concerning co-ordination number or morphology proved unreliable, possibly due to the similarity of Cu and Co (see the Supporting Information, Figure S9 and accompanying commentary), the large size of the particles making it hard to identify morphology changes, and the tendency of Cu especially to suffer artifacts associated with structural disorder (strain, vacancies, etc.) and thermal expansion, which both act to reduce the apparent coordination number. Nevertheless, the acquisition of EXAFS data under realistic conditions close to those typical in practical catalysis provides R-space data which is consistent with the results obtained by APXPS and NEXAFS measurements.

Materials. All chemicals were used as purchased. Standard Schlenk techniques were employed for NP synthesis.

Synthesis and ex Situ Characterization of 11 nm $Co_{50}Cu_{50}$ Nanoparticles: The metal precursor salts were dissolved in a reducing coordinating solvent (oleylamine) at 50 °C. $Co(acac)_2$ (27.0 mg, Aldrich, ≥99.0% pure) and $Cu(acac)_2$ (27.6 mg, Aldrich, 99.9% pure) were dissolved in oleylamine (5 mL, Aldrich) in a 50 mL round-bottom flask. The flask was pumped and subsequently flushed with Ar. The evacuation/

dx.doi.org/10.1021/jp405745n | J. Phys. Chem. C 2013, 117, 21803−21809

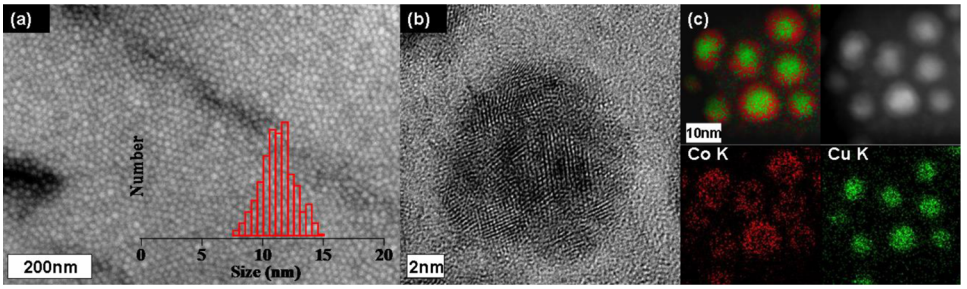

Figure 1. As synthesized $Co_{50}Cu_{50}$ nanopartlces: (a) SEM (overlaid with a histogram showing the particle size distribution counting over 200 particles); (b) HR-TEM images and (c) STEM/EDS phase-map spectra at Co and Cu K-edges (top left to bottom right, combined Co and Cu, TEM image of same region, Co only, Cu only).

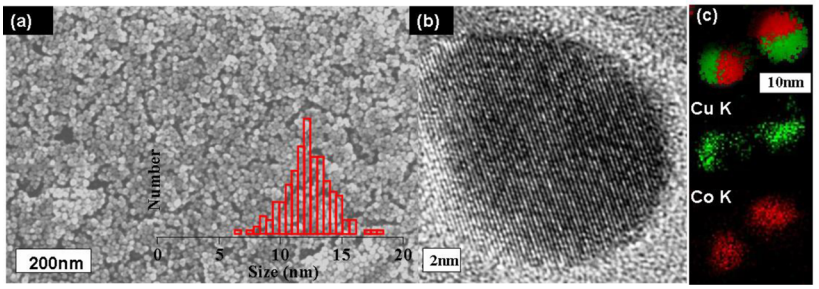

Figure 2. $Co_{50}Cu_{50}$ nanoparticles after redox conditioning at 350 °C: (a) SEM (overlaid with a histogram showing the particle size distribution counting over 200 particles); (b) HRTEM images showing single particle; and (c) STEM/EDS phase-mapping of Co and Cu K-edges of the two particles comined (top) and for just Cu (green) and Co (red) components respectively below.

purging cycle was repeated three times before the solution was purged by bubbling Ar for 15 min. Finally, the reaction flask was submerged in a molten salt bath preheated to 230 °C. The solution turned black in approximately 2 min, indicating the formation of colloidal particles. This colloidal suspension was then aged at 230 °C for 10 min prior to terminating the reaction by removing from the molten salt bath. The colloidal suspension was allowed to cool to room temperature before precipitating the nanoparticles with acetone, centrifugation, and redispersal in hexane. As synthesized nanoparticles were then stored in hexane until further use. 2D films of CoCu NPs were supported on Si wafers by dip-coating.

SEM and TEM pictures in Figure 1 indicate the formation of nanocrystalline NPs with a narrow size distribution (10.6 ± 1.3 nm) and it should be noted that the above synthesis conditions enable this result through the use of a high temperature nitrate salt bath to obtain and maintain a rapid and uniform heating environment during the reduction/conucleation.

STEM/EDS of a representative sample of the as-prepared NPs shows a bulk composition (probing over an area containing many particles) of 54 mol. % Cu. This is in good accordance with the expected 50:50 Co/Cu nominal composition. STEM/EDS analysis of 10 single particles from the same batch indicated their typical composition to be 55 ± 7 mol. % Cu, again in good agreement with the 50:50 nominal composition. This also demonstrates that both metals were present in similar concentrations in each single particle; that is, there is not a mix of particles, each of different composition, present. Figure 1c shows a STEM/EDS phase map at Co (red) and Cu (green) K lines indicating the formation of bimetallic NPs with Cu-rich cores and Co-rich shells. No stray monometallic NPs were detected.

STEM/EELS spectra obtained from the center and edge of a single as-prepared 50:50 alloy NP were also obtained (Supporting Information, Figure S1). The relative intensities of Co and Cu L-edge jumps indicate the formation of bimetallic copper-rich core/cobalt-rich shell nanoparticles, in agreement with STEM/EDS phase maps. Additionally, by comparing the metals with the O K-edge data it is noteworthy that the Co/O ratio is approximately 1 at the edge of the NP with significantly less overall contribution from O in the spectrum from the center of the NP where Cu dominates (although Co/O remains around 1). This indicates that in these as prepared nanoparticles the Co shells are oxidized, whereas the Cu-rich cores remained metallic (see the Supporting Information, Figure S1).

The powder X-ray diffraction (PXRD) pattern of the as-synthesized $Co_{50}Cu_{50}$ NPs (Supporting Information, Figure S2) shows a series of reflections commensurate with a face centered cubic (f.c.c.) phase with the (111) reflection centered at 2θ = 51.0° and higher reflections with 2θ values just below 60° and 90°. These appear to lie between those expected for fcc Co (51.7°, 60.4°, and 90.7°)[29] and fcc Cu (50.7°, 59. 3°, and 88.8°),[30] although have a slightly closer tendency to the Cu values. Moreover, a weak broad reflection at 2θ = ~43° likely corresponds to a CoO phase. Although this should not be overanalyzed in view of the data quality on our instrument, this is consistent with both the occurrence of Co and O together in the STEM/EELS spectra (as described above) and the possibility that the CoO is more amorphous than the metallic Cu rich core, which is thus dominant in the fcc diffraction pattern.

Conventional X-ray photoelectron spectroscopy (XPS) was also used to investigate the as-synthesized $Co_{50}Cu_{50}$ NPs based on the Co 2p and Cu 2p spectra (Figure S4). It was found that the near-surface region of the nanoparticles (~650 eV K.E. photoelectrons corresponding to a mean probing depth of ~15 Å) was 64 mol. % cobalt rich. Only 34 mol. % of the Co in this

dx.doi.org/10.1021/jp405745n | J. Phys. Chem. C 2013, 117, 21803−21809

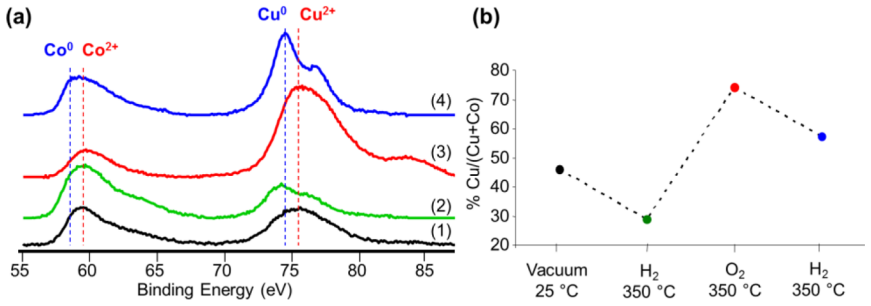

Figure 3. (a) Co and Cu 3p XP spectra using an incident photon energy of 380 eV and subjecting to a redox cycle: (1) 25 °C, in vacuum (black); (2) 350 °C 0.13 mbar H_2 (green); (3) 350 °C 0.13 mbar O_2 (red); and (4) 350 °C 0.13 mbar H_2 (blue). (b) Plot of % Cu at the surface (as a fraction of Cu+Co) as the conditions are cycled in panel a.

region was metallic, while 62 mol. % of the Cu was found to be metallic.

The combination of STEM/EDS, EELS and XPS demonstrate the "partially alloyed" nature of the as synthesized material. It is notable however that, thermodynamically, Cu is poorly soluble in Co with negligible miscibility expected for bulk systems below 500 °C.[31] It was previously shown for the Pt−Ru system, which exhibits a similarly large miscibility gap, that it is possible to produce a Pt−Ru alloy with mole concentrations different from those predicted by the thermodynamic phase diagrams.[32] Here, solid solutions beyond the binary solubility limit of Co and Cu have been synthesized at the nanoscale by colloidal chemical synthesis. We recently found that, for these as-prepared NPs, the surface structure could be strongly controlled by the temperature and the gas atmosphere to which they were exposed during APXPS.[33] However, we have found because these 'as prepared' materials exist only in a metastable state they cannot be used for detailed catalytic studies at higher pressures and temperatures as the material undergoes significant changes at temperature and in atmospheric pressure reactive gases. We therefore subjected the materials to a redox cycle procedure at 350 °C for 1 h in each of (1) 20% H_2, (2) 20% O_2, and (3) 20% H_2 in turn and at a total pressure of 1 bar (He balance). For the conditioned catalysts it is clear from the TEM (Figure 2) that no significant size or morphology change was observed; however, STEM/EDS phase-mapping (Figure 2c) reveals a bulk intraparticle phase segregation of Co and Cu to form contact dimer (Janus) particles. Since they do not change in average size, the dealloying seen must occur only within single particles so the overall composition remains the same. This is evidenced by the comparable areas of red (Co) and green (Cu) for the mapping of particles shown in Figure 2c. Crucially, they are also now relatively stable and can be exposed to reactive gases up to and above atmospheric pressure without any further shape changes, as shown in the Supporting Information.

In the subsequent section we investigate the structure and surface composition of these more stable forms using in situ X-ray spectroscopies. The use of these more stable dimer architectures is necessary to allow EXAFS and NEXAFS experiments at atmospheric pressure. Since we have previously found the time scale for substantial core−shell structure changes in nanoparticles of the non-redox treated kind shown in Figure 1 to be short relative to the time scales of these types of experiment,[33] it is reasonable to anticipate the surface structure will still be altered strongly by the temperature and by reactive gases, even after such intraparticle dealloying has occurred. For EXAFS measurements CoCu NP deposition in 3D oxide support materials (that more closely mimic typical catalysts) was conducted such that the final material contained a nominal 5 wt % CoCu loading in a MCF-17 (mesoporous silica) support. These were prepared via capillary inclusion as described elsewhere.[34]

RESULTS AND DISCUSSION

In order to gain molecular level insight under reactive gas atmospheres and catalytic reaction temperatures, we carried out in situ X-ray spectroscopic evaluation of the supported, redox-conditioned NPs (with dimer architectures) using APXPS (to determine the chemical composition of the topmost surface layers) soft X-ray based NEXAFS spectroscopy (to measure the oxidation states of Co and Cu near the surface) and hard X-ray EXAFS spectroscopy (to obtain the bonding and chemical structure of the bulk particles under redox gases and a CO_2/H_2 (1:3) reaction mixture).

APXPS of $Co_{50}Cu_{50}$ Dimer NPs. Co and Cu 3p APXP spectra were obtained using an incident photon energy of 380 eV as a compromise to maximize flux and obtain surface sensitivity by probing the topmost 0.8 nm (2−3 atomic layers) of a 2D film of NPs. A series of spectra for the $Co_{50}Cu_{50}$ NPs pretreated by redox cycling to form dimer NPs is shown in Figure 3a as the conditions are changed from vacuum, to 350 °C in 0.13 mbar H_2, O_2 and then H_2, in other words a full repeat of the original redox cycle but at lower gas pressures. The aim of this experiment is to get a qualitative impression of the changes and driving forces at play (as described elsewhere) and complement the higher pressure results obtained in the sections that follow by taking advantage of the greater surface sensitivity of photoelectron spectroscopy. Figure 3b shows the change in Cu/Co atomic ratio in this surface region at each step in the cycle. In vacuum, at 25 °C and in H_2 at 350 °C, the NPs exhibit a low surface concentration of Cu relative to Co (the H_2 treatment inducing further Co enrichment at the surface). Switching to oxygen brought Cu dramatically to the surface, as suggested previously for work on the qualitatively similar "as prepared particles" (not redox treated) this may in part be due to the kinetics of oxide formation between the two metals.[35] This is highlighted by the copper being oxidized, as indicated by the increased breadths and higher binding energy shifts of the Cu 3p features. On switching back to an H_2 environment, only some of the Co is returned to the surface indicating that this process is not fully reversible (Cu/Co atomic ratio of 1.4 rather than 0.37) at these pressures. This process was reproducible and could also be conducted without the initial H_2 treatment to produce the same final states as shown in the Supporting Information.

dx.doi.org/10.1021/jp405745n | J. Phys. Chem. C 2013, 117, 21803−21809

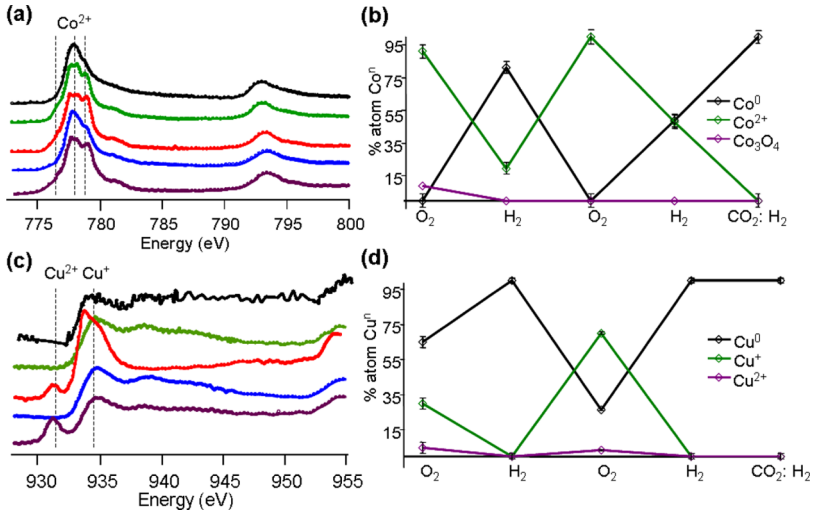

Figure 4. NEXAFS TEY spectra at (a) Co and (b) Cu L-edges under various conditions: 0.02 bar O_2 and 150 °C (purple), 0.02 bar H_2 and 150 °C (blue), 0.02 bar O_2 and 200 °C (red), 0.02 bar H_2 and 260 °C (green), and 2.7 bar CO_2/H_2 (1:3) and 260 °C (black). Vertical dashed lines indicate Co^{2+} and Cu^+, respectively. Panels b and d show the percentage of each metal present in the different forms based on the results of least-squares fitting of the spectra on the left to reference data (see the Supporting Information) for Co and Cu respectively in their different oxidation states based on the spectra in panels a and c.

In Situ NEXAFS Spectroscopy of $Co_{50}Cu_{50}$ Dimer NPs. The Co and Cu L-edge total electron yield (TEY) spectra, probing near surface regions up to ~2 nm in depth, were obtained under a series of redox conditions and then in situ during reaction of 1:3 CO_2/H_2 at 2.7 bar total pressure and 260 °C. The resulting spectra are shown in Figure 4, with the results of least squared fitting to reference data for the different oxidation states and at each condition also shown.

In broad terms changes between oxygen and hydrogen appear reversible on switching back and forth at 0.02 bar and increasing temperatures. The oxygen oxidizes Co and Cu partially while hydrogen is able to reduce the Cu and reduce a large fraction of the Co. In particular it should be noted that the presence of Cu appears to considerably decrease the temperature at which a large fraction of the Co atoms can be reduced in H_2. In these bimetallic NPs 80% of the Co atoms are found to be reduced in hydrogen at 150 °C while for previous similar studies on pure Co nanoparticles at similar (slightly higher) temperatures only 35% of the Co atoms were found to be reduced[36] (Figure S6). This is reminiscent of the effect seen with Pt (a very common Fischer−Tropsch promoter), which we have previously demonstrated also lowered the reduction temperature of Co in H_2 for CoPt NPs dramatically. The fact the reduction of Co is not complete is probably suggestive of some surface Co oxide, which cannot be fully removed under these pressure and temperature conditions (lower temperature than for APXPS). It is also notable that when exposed to O_2 (0.02 bar, 150 or 200 °C) Cu is present as Cu^{1+} and Cu^0, not Cu^{2+}; this indicates that copper is only mildly oxidized in these conditions.

For the spectra recorded in situ during reaction of CO_2/H_2 at 2.7 bar (also Figure 4) it can also be seen that Co atoms in the CoCu NPs were completely reduced under these reaction conditions. This effect could however be the effect of elevated H_2 partial pressure; see the Supporting Information for the dependence of pure Co nanoparticle reduction on H_2 pressure). Cu remains metallic, verifying that metallic Co and Cu are present under catalytically relevant temperatures (260 °C) and pressures (2.7 bar), similar to those in existing studies on CuCo.[2,4]

O K-edge spectra were also obtained for three conditions, O_2 treatment and then CO_2/H_2 reaction mixture (3:1) at increasing pressures (Figure 5). Although the spectra are

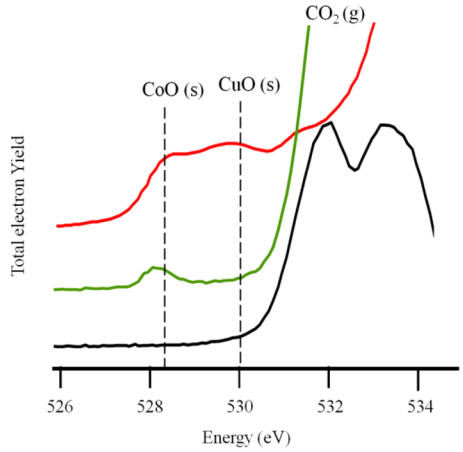

Figure 5. NEXAFS TEY spectra at O K-edge under various conditions: 0.02 bar O_2, 200 °C (red); 1 bar CO_2/H_2 (1:3) and 260 °C (green); and 2.7 bar CO_2/H_2 (1:3) and 260 °C (black). Vertical dashed lines indicate CoO and CuO, respectively, and the O−K edge features corresponding to gas phase species are considerably more intense and have been truncated to highlight the metal oxide features at lower energies.

dominated by gas phase O_2 and CO_2 (truncated) above around 530.5 eV, the spectra shown also contain features at lower photon energies. These can tentatively be assigned to metal oxides, as they have also been found to appear for the as-synthesized nanoparticles, measured in He, where electron microscope (vacuum) based techniques have confirmed metal oxides are expected to be present. For the spectrum in O_2 at 200 °C (red) a broad oxide peak is seen, however, under the CO_2/H_2 reaction 1 bar at 260 °C total pressure the low energy peak at 528 eV remained, but the 530 eV component vanished

dx.doi.org/10.1021/jp405745n | J. Phys. Chem. C 2013, 117, 21803−21809

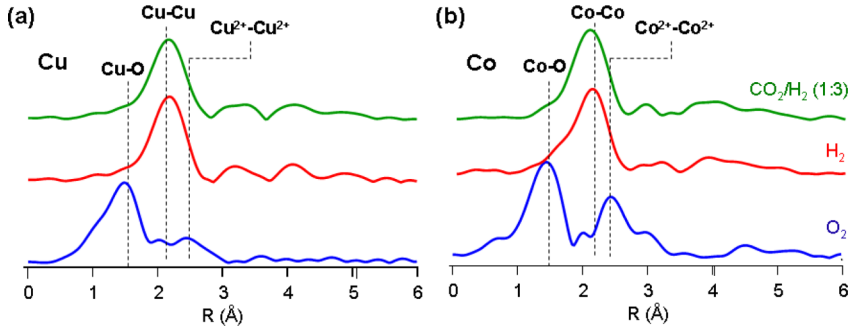

Figure 6. 6k^3-weighted EXAFS oscillations for (a) Co and (b) Cu at 350 °C and under various conditions: 0.02 bar O_2 (blue), 0.02 bar H_2 (red), and 1 bar CO_2/H_2 (1:3). Vertical dashed lines indicate Co(Cu)−O, $Co^0(Cu^0)$−$Co^0(Cu^0)$, and $Co^{2+}(Cu^{2+})$−$Co^{2+}(Cu^{2+})$ near neighbor shells/distances, respectively.

(about 0.75 bar partial pressure of H_2). On further increasing the total pressure to 2.7 bar (partial pressures of H_2 about 2 bar), all traces of metal oxides disappeared from the spectra. In agreement with the aforementioned relative reducibility of the metals obtained from the respective metal L-edges, the low energy peak at 528 eV was assigned to CoO_x and the high energy shoulder at 530 eV to CuO_x.

NEXAFS TEY spectra could be obtained in 4 bar of H_2 using our flow reaction cell, as also demonstrated for 10 nm Co NPs (Figure S7); however, CO_2 (or CO) pressures above 1 bar seemed to be limiting the TEY signal due to increased background absorption and ionization which are challenging to overcome and a possibly serious limitation in the application of this technique to higher pressure reactions. This can be seen in the shape of the CO_2(g) feature at higher CO_2 pressures in Figure 5 (black), where the peak is being split at its center by gas phase absorption effects.

Local Bonding Environment of $Co_{50}Cu_{50}$ Dimer NPs via In Situ EXAFS. For 11 nm particles, a large fraction (around 50%) of the atoms are 'near surface' in that they reside in the surface most 2 nm of the NPs. Accordingly, XAFS fluorescence yield (FY) spectroscopy, although usually considered a bulk measurement, is in this case still a surface sensitive probe of the local bonding and chemical structure in these types of NPs. The Co and Cu K-edge XAFS (FY) spectra were obtained under various conditions, and the results for the k^3-weighed EXAFS oscillations in R-space are displayed in Figure 6. Only metallic Co and Cu were observed at 350 °C under both the reducing conditions (0.02 bar H_2) and the reaction conditions (CO_2 hydrogenation, CO_2: H_2 = 1:3 and p_{H_2} = 0.75 bar).

When oxidized under 0.02 bar O_2 at 350 °C, the 3D nanoparticle catalyst (in MCF-17) showed two near neighbor shells: a lower-R shell for the metal-oxide bonding and a higher-R shell for the (oxidized) metal−metal bonding, indicating fully oxidized Co and Cu (Figure 6). Upon reduction in H_2 (350 °C), both Co and Cu were reduced back to the metallic states and remained metallic during the catalytic reaction of CO_2 in H_2 on the nanoparticles. This is in good agreement with the NEXAFS data obtained above.

CONCLUSIONS

By developing a synthetic route to form $Cu_{50}Co_{50}$ NPs of 11 nm in diameter and stabilizing them via redox treatments to withstand the conditions used for catalysis without undergoing further irreversible changes, we have been able to study the surface oxidation and metal segregation effects in situ for CoCu NPs in reducing, oxidizing, and reaction mixture gases for the reaction of CO_2 with H_2. In O_2 both metals are significantly oxidized and Cu segregates to the surface in the Cu^+ state. In H_2 this segregation is reversed, with Co coming to the surface; the majority of Co atoms being probed are reduced and Cu is fully reduced. The reduction of Co in the CoCu NPs in H_2 notably also occurs at much lower temperatures than were previously identified to be necessary for pure Co NPs. The extent of this reduction may also be dependent on the pressure of H_2 as is shown in the case for pure Co NPs. Reversible surface segregation and oxidation of NPs that occurs under reaction conditions is especially important for their application as heterogeneous catalysts, which have long been known to depend strongly on the surface composition and oxidation state. Accordingly in situ X-ray spectroscopy studies of these CoCu NPs were also carried out under reaction conditions for the CO_2/H_2 reaction, which showed that both Co and Cu are maintained in a fully reduced oxidation state during the reaction, despite the potential for oxidation by water produced during reaction.

ASSOCIATED CONTENT

Supporting Information

STEM/EELS spectra, XRD data, XPS spectra, additional APXPS and NEXAFS data, and simulations of Cu and Co EXAFS. This information is available free of charge via the Internet at http://pubs.acs.org.

AUTHOR INFORMATION

Corresponding Author

*Tel: (510) 642-4053. E-mail: somorjai@berkeley.edu.

Present Address

[▽]Department of Chemistry, Durham University, South Road, Durham, DH1 3LE United Kingdom.

Author Contributions

[#]These authors contributed equally.

Notes

The authors declare no competing financial interests.

ACKNOWLEDGMENTS

The user projects in the Advanced Light Source and Molecular Foundry at the Lawrence Berkeley National Laboratory were supported by the Director, Office of Energy Research, Office of Basic Energy Sciences of the U.S. Department of Energy under Contract DE-AC02-05CH11231. We acknowledge Honda Research Institute, USA for the financial support.

REFERENCES

(1) de Klerk, A. Fischer–Tropsch Fuels Refinery Design. *Energy Environ. Sci.* **2011**, *4* (4), 1177–1205.

(2) Chanenchuk, C. A.; Yates, I. C.; Satterfield, C. N. The Fischer–Tropsch Synthesis with a Mechanical Mixture of a Cobalt Catalyst and a Copper-Based Water Gas Shift Catalyst. *Energy Fuels* **1991**, *5* (6), 847–855.

(3) Mo, X. H.; Tsai, Y. T.; Gao, J.; Mao, D. S.; Goodwin, J. G. Effect of Component Interaction on the Activity of Co/CuZnO for CO Hydrogenation. *J. Catal.* **2012**, *285* (1), 208–215.

(4) Nerlov, J.; Sckerl, S.; Wambach, J.; Chorkendorff, I. Methanol Synthesis from CO_2, CO and H-2 over Cu(100) and Cu(100) Modified by Ni and Co. *Appl. Catal. A, Gen.* **2000**, *191* (1–2), 97–109.

(5) Smith, M. L.; Kumar, N.; Spivey, J. J. CO Adsorption Behavior of Cu/SiO2, Co/SiO2, and CuCo/SiO_2 Catalysts Studied by In Situ DRIFTS. *J. Phys. Chem. C* **2012**, *116* (14), 7931–7939.

(6) Wang, J. J.; Chernavskii, P. A.; Khodakov, A. Y.; Wang, Y. Structure and Catalytic Performance of Alumina-Supported Copper-Cobalt Catalysts for Carbon Monoxide Hydrogenation. *J. Catal.* **2012**, *286*, 51–61.

(7) Courty, P.; Durand, D.; Freund, E.; Sugier, A. C-1-C-6 Alcohols from Synthesis Gas on Copper Cobalt Catalysts. *J. Mol. Catal.* **1982**, *17* (2–3), 241–254.

(8) Buess, P. C., R. F. I.; Frennet, A.; Ghenne, E.; Hubert, C.; Kruse, N. *Co-Precipitated Catalysts for Fischer–Tropsch Synthesis* **2002**.

(9) Waugh, K. C. Methanol Synthesis. *Catal. Today* **1992**, *15* (1), 51–75.

(10) Khodakov, A. Y.; Chu, W.; Fongarland, P. Advances in the Development of Novel Cobalt Fischer–Tropsch Catalysts for Synthesis of Long-Chain Hydrocarbons and Clean Fuels. *Chem. Rev.* **2007**, *107* (5), 1692–1744.

(11) van Santen, R. A.; Ghouri, M. M.; Shetty, S.; Hensen, E. M. H. Structure Sensitivity of the Fischer–Tropsch Reaction; Molecular Kinetics Simulations. *Catal. Sci. Technol.* **2011**, *1* (6), 891–911.

(12) Spivey, J. J.; Egbebi, A. Heterogeneous Catalytic Synthesis of Ethanol from Biomass-Derived Syngas. *Chem. Soc. Rev.* **2007**, *36* (9), 1514–1528.

(13) Grabow, L. C.; Mavrikakis, M. Mechanism of Methanol Synthesis on Cu through CO_2 and CO Hydrogenation. *ACS Catal.* **2011**, *1* (4), 365–384.

(14) Fujitani, T.; Nakamura, I.; Uchijima, T.; Nakamura, J. The Kinetics and Mechanism of Methanol Synthesis by Hydrogenation of CO_2 over a Zn-Deposited Cu(111) Surface. *Surf. Sci.* **1997**, *383* (2–3), 285–298.

(15) Van der Laan, G. P.; Beenackers, A. Kinetics and Selectivity of the Fischer–Tropsch Synthesis: A Literature Review. *Catal. Rev.-Sci. Eng.* **1999**, *41* (3–4), 255–318.

(16) Storsaeter, S.; Chen, D.; Holmen, A. Microkinetic Modelling of the Formation of C-1 and C-2 Products in the Fischer–Tropsch Synthesis over Cobalt Catalysts. *Surf. Sci.* **2006**, *600* (10), 2051–2063.

(17) Somorjai, G. A.; Park, J. Y. Molecular Factors of Catalytic Selectivity. *Angew. Chem.-Int. Ed.* **2008**, *47* (48), 9212–9228.

(18) Somorjai, G. A.; Beaumont, S. K.; Alayoglu, S. Determination of Molecular Surface Structure, Composition, and Dynamics under Reaction Conditions at High Pressures and at the Solid-Liquid Interface. *Angew. Chem.-Int. Ed.* **2011**, *50* (43), 10116–10129.

(19) Salmeron, M.; Schlogl, R. Ambient Pressure Photoelectron Spectroscopy: A New Tool for Surface Science and Nanotechnology. *Surf. Sci. Rep.* **2008**, *63* (4), 169–199.

(20) Gunter, M. M.; Bems, B.; Schlogl, R.; Ressler, T. In Situ Studies on the Structure of Copper Oxide/Zinc Oxide Catalysts. *J. Synchrotron Radiat.* **2001**, *8*, 619–621.

(21) de Smit, E.; de Groot, F. M. F.; Blume, R.; Havecker, M.; Knop-Gericke, A.; Weckhuysen, B. M. The Role of Cu on the Reduction Behavior and Surface Properties of Fe-Based Fischer–Tropsch Catalysts. *Phys. Chem. Chem. Phys.* **2010**, *12* (3), 667–680.

(22) de Smit, E.; Beale, A. M.; Nikitenko, S.; Weckhuysen, B. M. Local and Long Range Order in Promoted Iron-Based Fischer–Tropsch Catalysts: A Combined In Situ X-ray Absorption Spectroscopy/Wide Angle X-ray. *J. Catal.* **2009**, *262* (2), 244–256.

(23) Chinchen, G. C.; Denny, P. J.; Parker, D. G.; Short, G. D.; Spencer, M. S.; Waugh, K.; Whan, D. A. The Activity of Cu-ZnO-Al_2O_3 Methanol Synthesis Catalysts. *Abstr. Pap. Am. Chem. Soc.* **1984**, *188* (Aug), 17 Fuel..

(24) Iglesia, E. Design, Synthesis, and Use of Cobalt-Based Fischer–Tropsch Synthesis Catalysts. *Appl. Catal. A, Gen.* **1997**, *161* (1–2), 59–78.

(25) Grass, M. E.; Karlsson, P. G.; Aksoy, F.; Lundqvist, M.; Wannberg, B.; Mun, B. S.; Hussain, Z.; Liu, Z. New Ambient Pressure Photoemission Endstation at Advanced Light Source Beamline 9.3.2. *Rev. Sci. Instrum.* **2010**, *81*, (5).

(26) Zheng, F.; Alayoglu, S.; Guo, J. H.; Pushkarev, V.; Li, Y. M.; Glans, P. A.; Chen, J. L.; Somorjai, G. In-situ X-ray Absorption Study of Evolution of Oxidation States and Structure of Cobalt in Co and CoPt Bimetallic Nanoparticles (4 nm) under Reducing (H-2) and Oxidizing (O-2) Environments. *Nano Lett.* **2011**, *11* (2), 847–853.

(27) Marcus, M. A.; MacDowell, A. A.; Celestre, R.; Manceau, A.; Miller, T.; Padmore, H. A.; Sublett, R. E. Beamline 10.3.2 at ALS: a Hard X-ray Microprobe for Environmental and Materials Sciences. *J. Synchrotron Radiat.* **2004**, *11*, 239–247.

(28) Ravel, B.; Newville, M. ATHENA, ARTEMIS, HEPHAESTUS: Data Analysis for X-ray Absorption Spectroscopy Using IFEFFIT. *J. Synchrotron Radiat.* **2005**, *12*, 537–541.

(29) Owen, E. A.; Jones, D. M. Effect of Grain Size on the Crystal Structure of Cobalt. *P Phys Soc Lond B* **1954**, *67* (414), 456–466.

(30) Otte, H. M. Lattice Parameter Determinations with an X-Ray Spectrogoniometer by Debye-Scherrer Method and Effect of Specimen Condition. *J. Appl. Phys.* **1961**, *32* (8), 1536.

(31) *ASM Handbook*; Alloy Phase Diagrams. ASM International: OH, 1992; Vol. 3.

(32) Hills, C. W.; Mack, N. H.; Nuzzo, R. G. The Size-Dependent Structural Phase Behaviors of Supported Bimetallic (Pt-Ru) Nanoparticles. *J. Phys. Chem. B* **2003**, *107* (12), 2626–2636.

(33) Tao, F.; Grass, M. E.; Zhang, Y. W.; Butcher, D. R.; Renzas, J. R.; Liu, Z.; Chung, J. Y.; Mun, B. S.; Salmeron, M.; Somorjai, G. A. Reaction-Driven Restructuring of Rh-Pd and Pt-Pd Core-Shell Nanoparticles. *Science* **2008**, *322* (5903), 932–934.

(34) Rioux, R. M.; Song, H.; Hoefelmeyer, J. D.; Yang, P.; Somorjai, G. A. High-Surface-Area Catalyst Design: Synthesis, Characterization, and Reaction Studies of Platinum Nanoparticles in Mesoporous SBA-15 Silica. *J. Phys. Chem. B* **2005**, *109* (6), 2192–2202.

(35) Beaumont, S. K.; Alayoglu, S.; Pushkarev, V. V.; Liu, Z.; Kruse, N.; Somorjai, G. A. Exploring Surface Science and Restructuring in Reactive Atmospheres of Colloidally Prepared Bimetallic CuNi and CuCo Nanoparticles on SiO_2 In Situ Using Ambient Pressure X-ray Photoelectron Spectroscopy. *Faraday Discuss.* **2013**, *162*, 31–44.

(36) Iablokov, V.; Beaumont, S. K.; Alayoglu, S.; Pushkarev, V. V.; Specht, C.; Gao, J. H.; Alivisatos, A. P.; Kruse, N.; Somorjai, G. A. Size-Controlled Model Co Nanoparticle Catalysts for CO_2 Hydrogenation: Synthesis, Characterization, and Catalytic Reactions. *Nano Lett.* **2012**, *12* (6), 3091–3096.